The Journal of Physical Chemistry A

 VOLUME 101, NUMBER 3, JANUARY 16, 1997

ARTICLES

Classical Variational Transition State Theory Study of Hydrogen Atom Diffusion Dynamics in Imperfect Xenon Matrices

Ran Pan and Lionel M. Raff*

Department of Chemistry, Oklahoma State University, Stillwater, Oklahoma 74078

Received: July 23, 1996; In Final Form: November 1, 1996[⊗]

Thermal diffusion rates of hydrogen atoms in imperfect face-centered-cubic (fcc) xenon lattices containing up to 4.12% vacant sites have been computed using classical Monte Carlo variational transition state theory with a pairwise Xe/H interaction potential obtained from the results of *ab initio* calculations at the MP4-(SDTQ) level of theory. Convergence of the required integrals is achieved by combining importance sampling and a damped trajectory procedure with the standard Markov walk. The variational flux through spherical dividing surfaces is minimized as a function of radius of the dividing surface. The results show that the presence of 1.4% vacant lattice sites lowers the diffusion barrier by about 0.006 eV relative to the perfect fcc crystal system. The computed values of the hydrogen atom diffusion coefficients at 40 K indicate that, over the range of vacancies considered, the diffusion coefficients increase exponentially with the percentage of the lattice vacancies. The calculations also show that the lattice vacancies are mobile. The studies reveal that the propensity for vacant site mobility increases as the total number of lattice vacancies increases. Since this effect decreases the potential barrier to diffusion, the diffusion coefficients obtained from the variational transition state theory calculation are lower limits for a system with the present interaction potential. The calculated diffusion coefficients indicate that experimental matrices vapor-deposited at 10 and 28 K contain about 1.8 and 1.2% vacant sites, respectively. Since the calculated diffusion rates are lower limits, these percentages are upper limits for the potential surface used in the present investigation.

I. Introduction

In matrix isolation experiments, the low-temperature, constrained environment of the matrix cage serves to moderate fast reactions that are typically characterized by low activation energies. Example include rotational isomerizations, radical recombination processes, and highly exothermic reactions. This moderating effect increases the half-life and permits a variety of experimental measurements to be made. Pimentel and co-workers[1,2] observed IR-induced rotational isomerization of HONO in a nitrogen matrix at 20 K. Thermally activated rotational interconversion has been observed for aldehyde−ketene systems in Ar at 30 K[3] and for cyclohexane,[4] methanol,[5] ethylene glycol,[6] and haloethanols[7,8] in inert, low-temperature matrices. Most recently, Benderskii and Wight[9] have reported thermal rate measurements for rotational isomerization of *trans*-1,2-difluoroethane in Ar matrices between 30 and 36 K. This process has also been investigated both experimentally[10,11] and theoretically[12−14] by Günthard and co-workers. The bimolecular addition of F_2 to ethylene is an example of a highly exothermic process whose study is facilitated by the matrix environment.[15−20]

The conformational inversion of *cis*- and *trans*-HONO under matrix-isolated conditions have been investigated in detail by Agrawal *et al.*[21,22] These investigations have shown that, in addition to providing cage effects, the matrix environment plays

[⊗] Abstract published in *Advance ACS Abstracts*, January 1, 1997.

S1089-5639(96)02215-3 CCC: $14.00

a significant role in the reaction mechanism. It is found that both the *cis* → *trans* and *trans* → *cis* isomerization rates are enhanced by the presence of the matrix in spite of the steric effects produced by the environment. By comparison to gas-phase data, Agrawal *et al.*[21,22] demonstrated that this enhancement occurs because the matrix opens a (vibration → lattice phonon → rotation → torsional vibration) energy transfer pathway. The intramolecular vibrational relaxation rates in the matrix are found to be slow relative to the isomerization rates. Hence, the dynamics are nonstatistical. The presence of lattice vacancies is found to exert a profound influence upon the dynamics. When the percentage of vacancies reaches 20%, the calculated dynamics in the matrix approach the gas-phase results. In the gas phase, deuterium and ^{18}O isotopic substitutions have very little effect upon the rates.[22] In the matrix, however, a significant isotope effect is obtained which is attributed to a reduced rate of energy transfer from the lattice to rotation of DONO and $H^{18}ON^{18}O$ due to the increased moment of inertia. That is, isotopic substitution creates an energy transfer bottleneck in the proposed (vibration → lattice phonon → rotation → torsional vibration) mechanism.

Mobility and diffusion often play critical roles in reactions occurring under matrix-isolation conditions. The importance of these effects becomes obvious when the matrix is used as a means for containing high-energy density materials. In spite of this importance, only a few experimental and theoretical studies of such processes have been reported. Feld, Kunttu, and Apkarian[23] have carried out measurements of fluorine atom mobilities in an argon matrix subsequent to photodissociation while Lawrence and Apkarian[24] have measured the mobility of photoexcited oxygen atoms in Xe lattices. Krueger and Weitz[25] have reported measurements of oxygen atom recombination rates in Xe matrices. LaBrake and Weitz[26] have obtained data for hydrogen atom diffusion in Xe matrices at 40 K. Misochko *et al.*[27] were able to demonstrate that direct UV photolysis of C_2H_4:F_2 complexes at 14 K forms 1,2-difluoroethane in doubly substitutional sites, whereas the diffusion-limited reaction of fluorine atoms with isolated C_2H_4 molecules at 25 K leads to 1,2-difluoroethane in singly substitutional sites. Theoretical studies of atomic diffusion in rare-gas matrices have been reported by Ford *et al.*[28] for oxygen atoms diffusing in perfect face-centered-cubic (fcc) xenon matrices between 32 and 80 K. Perry *et al.*[29] have used classical variational transition state theory to examine hydrogen atom diffusion and tunneling in perfect fcc Xe matrices between 12 and 80 K. This system has also been investigated by Guo and Thompson,[30] who employed simple transition-state theory with an empirical potential to compute the hydrogen atom diffusion rates.

In all cases, the measured diffusion rates[25,26] exceed the values computed for a perfect fcc rare-gas lattice[28−30] by several orders of magnitude. These differences have led to the suggestion that the enhanced diffusion rates obtained in the experiments are due to the presence of vacancies in the experimental matrices.[28,29] The presence of such vacancies is also suggested by the experimental results reported by LaBrake and Weitz.[26] These investigators found that hydrogen diffusion rates at 40 K were greater in Xe matrices vapor-deposited at 10 K than in those deposited at 28 K and then warmed to 40 K. The inference is that there exists a larger number of vacancies in the lattice deposited at 10 K that are not annealed by warming to 40 K. Clearly, the presence of lattice vacancies can play a major role in the processes taking place within the matrix. The rotational isomerization of HONO[21,22] and the mechanism for the F_2:C_2H_4 matrix reaction[20,31] as well as diffusion processes are examples.

In the present paper, we report the results of a classical variational transition state theory investigation of hydrogen atom diffusion in imperfect xenon matrices that contain a varying percentage of lattice vacancies. The results show that the diffusion rate increases exponentially with percentage of lattice vacancies so long as the percentage of vacancies is small. We also find that lattice vacancies in this system are mobile and that this effect serves to increase the atom diffusion rate.

II. Matrix Model and Computational Methods

The matrix model used in the present study is the ($5 \times 5 \times 5$) fcc lattice of 125 unit cells containing 666 lattice atoms previously described by Raff.[20] This model has been found to be sufficiently large to accurately represent the density and volume expansion upon trapping of 1,2-difluoroethane.[20] In order to represent bulk effects upon energy transfer that would be present for an infinite lattice model, the velocity reset method developed by Riley *et al.*[32] is employed. To do so, the 666 lattice atoms are first divided into three discrete zones. This division is determined once the size of the lattice model has been chosen using density, volume expansion, or other criteria. The boundary zone (B zone) comprises the atoms located on the boundary of the crystal. There are 302 such atoms in the present case. The positions of these lattice atoms are fixed. Their presence reduces edge effects and maintains the desired lattice symmetry. The secondary zone (Q zone) contains the 302 lattice sites within one unit cell distance of the outer boundary. The solution of Hamilton's equations for the motion of these atoms is modified by the reset functions associated with each atom in the Q zone.[32] This procedure maintains the temperature of the lattice as energy is removed or inserted by the chemical or physical processes that are occurring. The primary zone (P zone) comprises the remaining atoms (62 in the present case) of the crystal. The motions of these atoms are affected only by the forces produced by the interaction potential.

We simulate an imperfect lattice containing n vacancy sites by starting with the perfect fcc lattice as described above. Lattice vacancies are then created in the P and Q zones by random removal of n lattice atoms. The initial state is prepared by placing the hydrogen atom at the most stable absorption site within the innermost unit cell of the ($5 \times 5 \times 5$) matrix. Often this position is at the geometric center of the cell. However, because of the existence of n vacancies in the crystal, the lattice symmetry is destroyed. This may change the location of the most stable absorption site.

The objective of the present study is to calculate the hydrogen atom diffusion rate to an adjacent site, which, in a fixed fcc matrix, would be located at the midpoint of an edge of the center unit cell. Although the existence of vacancies introduces deviations from the expected symmetry, it is assumed that such deviations may be ignored in the computation of the jump frequency between adsorption sites. That is, the diffusion distance, d, between sites in the imperfect lattice is taken to be identical to that for the perfect fcc crystal. Because the ratio of hydrogen atoms to the number of adsorption sites is small, the diffusion coefficient at temperature T, $D(T)$, can be related to the jump frequency, $k(T)$, by

$$D(T) = [d^2 k(T) f]/\alpha \qquad (1)$$

where f is the fraction of vacant sites ($f = 1$ here) and α is the dimensionally factor, which is three in the present case since diffusion within the matrix is three-dimensional.

In classical variational transition-state theory, the jump frequency is approximated by the flux, $F(T)$, across a theoretical

dividing surface separating the two adsorption sites. If the system behaves statistically, this flux must be an upper limit to the actual diffusion rate since all diffusion events involve crossing of the dividing surface, but not all crossings result in diffusion. Consequently, we seek the dividing surface that minimizes the flux. For a canonical system, the jump frequency is proportional to the probability of the hydrogen atom being on the dividing surface and to the velocity of the atom perpendicular to that surface. Thus, $F(T)$ can be expressed by the sum of all such products averaged over the phase space of the system divided by the total available phase-space volume. This is,

$$F(T) = \frac{\int_p\int_q \exp(-E/k_bT)|V_\pm|\delta(q-q_c)\prod_{\substack{i=1\\ i\neq k}}^{3N} dq_i\, dp_i}{\int_p\int_q \exp(-E/k_bT)\prod_{\substack{i=1\\ i\neq k}}^{3N} dq_i\, dp_i} \quad (2)$$

where the delta function, $\delta(q - q_i)$, is unity when on the dividing surface and zero otherwise. In eq 2, E is the total system energy and k_b is the Boltzmann constant. The configuration space integrals cover the space corresponding to reactant conformations. For the present system, E is given by

$$E = \sum_{\substack{i=1\\ i\neq k}}^{N} [p_{xi}{}^2 + p_{yi}{}^2 + p_{zi}{}^2]/2m_i + [p_{xH}{}^2 + p_{yH}{}^2 + p_{zH}{}^2]/2m_H + V_T \quad (3)$$

where p_{qi} ($q = x, y, z$) represents the momentum of the lattice atom i in the q direction and V_T is the total system potential energy. The subscript runs over all lattice atoms except the vacancy positions, k, and "H" denotes the hydrogen atom.

We have previously utilized spherical and cubical dividing surfaces to minimize $F(T)$ and found that spherical surfaces generally yield the lower flux.[28] For both spherical and cubical dividing surfaces, the integrations over momenta in eq 2 can be done analytically. Such integration yields

$$F(T) = \langle v\rangle \frac{\int_q \exp(-V_T/k_bT)\delta(q-q_c)\prod_{\substack{i=1\\ i\neq k}}^{3N} dq_i}{\int_q \exp(-V_T/k_bT)\prod_{\substack{i=1\\ i\neq k}}^{3N} dq_i} \quad (4)$$

where $\langle v\rangle$ represents the average velocity of the hydrogen atom.

If the potential being employed is separable into a lattice potential plus a hydrogen−lattice interaction, eq 4 may be written in the form

$$F(T) = \langle v\rangle \frac{\int_q \exp(-V_M/k_bT)\exp(-V_I/k_bT)\delta(q-q_c)\prod_{\substack{i=1\\ i\neq k}}^{3N} dq_i}{\int_q \exp(-V_M/k_bT)\exp(-V_I/k_bT)\prod_{\substack{i=1\\ i\neq k}}^{3N} dq_i} \quad (5)$$

where the V_M and V_I are the lattice potential and the hydrogen−lattice interaction, respectively, and

$$V_T = V_I + V_M \quad (6)$$

The complexity of the potential precludes analytical evaluation of eq 5. We therefore utilize Monte Carlo methods to execute the required integrations. A Metropolis sampling procedure is employed in which the dividing surface is replaced with a dividing "slab" of width Δw. If Δw is sufficiently small that the integrand of eq 5 is constant across the width, eq 5 becomes

$$F(T) = [\langle v\rangle/\Delta w] \frac{\int_q \exp(-V_M/k_bT)\exp(-V_I/k_bT)\delta(\Delta w)\prod_{\substack{i=1\\ i\neq k}}^{3N} dq_i}{\int_q \exp(-V_M/k_bT)\exp(-V_I/k_bT)\prod_{\substack{i=1\\ i\neq k}}^{3N} dq_i} \quad (7)$$

where $\delta(\Delta w)$ is unity if a configuration point lies within the dividing slab and zero otherwise. In principle, eq 7 may be evaluated using a random set of M points in the multidimensional configuration space of the system. For such a randomly selected set of points, the Monte Carlo approximant for eq 7 is

$$F(T) = [\langle v\rangle/\Delta w] \frac{\sum_i^M [\exp(-V_M/k_bT)\exp(-V_I/k_bT)\delta(\Delta w)]_i}{\sum_i^M [\exp(-V_M/k_bT)\exp(-V_I/k_bT)]_i} \quad (8)$$

Although eq 8 yields the flux across the dividing slab, its convergence rate will be extremely slow if totally random points are selected for all atoms since virtually all points selected will correspond to highly improbable configurations. The situation may be improved by selecting the points from a Markov walk weighted by the canonical distribution function $\exp[-V_T/kT]$. In this case, the flux will be given by

$$F(T) \approx [\langle v\rangle/\Delta w]\sum_i^M [\delta(\Delta w)]_i \quad (9)$$

The convergence rate of eq 9 will be significantly greater than that of eq 8. However, convergence will still be very slow due to the infrequency of sampling in the regions of high potential. A more satisfactory convergence rate may be obtained by using a Markov walk weighted by the canonical distribution function for the lattice alone, $\exp[-V_M/kT]$. For such a selection method,

$$F(T) \approx 0.5[\langle v\rangle/\Delta w] \frac{\sum_i^M [\exp(-V_I/k_bT)\delta(\Delta w)]_i}{\sum_i^M [\exp(-V_I/k_bT)]_i} \quad (10)$$

where a factor of 0.5 is included to correct for entries into the dividing volume from the wrong direction. Equation (10) has previously been used to compute silicon and hydrogen atom diffusion rates on Si(111) and Si(111)-(7 × 7) surfaces.[33]

The convergence rate by eq 10 is still very slow although it can be used to obtain diffusion rates on surfaces and in matrices. Typically, millions of Markov steps are required for surface diffusion. For matrices at cryogenic temperatures, convergence is even slower. A new method has been proposed by Ford *et*

al.[28] to circumvent this problem. The method is based on the assumption that the major contribution to $F(T)$ in eq 7 arises from configurations in the neighborhood of the minimum-energy pathway for the diffusion process. These configurations can be conveniently located and sampled using a combination of canonical Markov moves on the lattice atoms and totally random moves on the embedded hydrogen atom followed by a series of damped trajectory cycles in which the lattice is allowed to relax toward its minimum-energy configuration in the field of a stationary hydrogen atom.[20,28,31] When this procedure was employed, the Monte Carlo integrations were observed to converge at a much greater rate since all of the sampling was done in statistically important regions of configuration space near the minimum-energy path.[28]

For spherical dividing surfaces, it is convenient to write eq 7 in the form

$$F(T) \approx [\langle c \rangle/\Delta w][\int_q \exp(-V_M/k_bT) \times \exp(-V_I/k_bT)\delta(\Delta w)\prod_{\substack{i=1\\ i\neq k}}^{3N} dq_i\, {r_H}^2\, dr_H \times \sin\theta_H\, d\theta_H\, d\phi_H]/[\int_q \exp(-V_M/k_bT)\exp(-V_I/k_bT)\prod_{\substack{i=1\\ i\neq k}}^{3N} dq_i \times {r_H}^2\, dr_H \sin\theta_H\, d\theta_H\, d\phi_H] \quad (11)$$

where hydrogen atom coordinates are separated and expressed in a spherical system. The Monte Carlo approximant for eq 11 is similar in form to eq 8. It is

$$F(T) \approx [1/(2 \times 12 \times \Delta r)](8k_bT/\pi M_H)^{1/2} \times \frac{\sum_i^M [\exp(-V_M/k_bT)\exp(-V_I/k_bT){r_H}^2\delta(\Delta w)]_i}{\sum_i^M [\exp(-V_M/k_bT)\exp(-V_I/k_bT){r_H}^2]_i} \quad (12)$$

where the terms under the summations are evaluated after every Markov step on the lattice and after every damped trajectory cycle. In eq 12, Δr is the width of the dividing spherical slab and M_H is the hydrogen atom mass. The factor of 2 corrects for surface crossings in the wrong direction. The factor of 12 removes the degeneracy in the calculation which is present since a spherical dividing surface counts jumps to 12 equivalent diffusion sites. If the Markov walk is weighted by the canonical distribution function for the lattice alone, the Monte Carlo approximant for eq 11 becomes

$$F(T) \approx [2 \times 12 \times \Delta r]^{-1}(8k_bT/\pi M_H)^{1/2} \times \frac{\sum_i^M [\exp\{-V_I/k_bT\}{r_H}^2\delta(\Delta w)]_i}{\sum_i^M [\exp\{-V_I/k_bT\}{r_H}^2]_i} \quad (13)$$

In practice, the Markov walk is executed by moving m randomly selected lattice atoms ($7 \leq m \leq 20$) and the hydrogen atom in each step of the walk. The lattice atoms are moved according to

$$q_i^{new} = q_i^{old} + \xi_i \Delta q \quad (i = 1, 2, 3, ..., m) \quad (14)$$

where q_i^{new} and q_i^{old} are the new and old x, y, and z coordinates of the lattice atom i, respectively, and Δq is the Markov step size. The ξ_i are random numbers selected from a uniform distribution on the interval [0.1]. For the hydrogen atom,

$$\Delta x_H = \Delta Q \sin\theta_H \cos\phi_H \quad (15)$$

$$\Delta y_H = \Delta Q \sin\theta_H \sin\phi_H \quad (16)$$

$$\Delta z_H = \Delta Q \cos\phi_H \quad (17)$$

where

$$\theta_H = \cos^{-1}[1 - 2\xi_{H1}] \quad (18)$$

$$\theta_H = 2\pi\xi_{H2} \quad (19)$$

$$\Delta Q = \Delta q \xi_{H3} \quad (20)$$

The values of m and Δq are adjusted to produce a near-unit ratio between accepted and rejected moves. In most cases, $m = 7$ and Δq is 0.0866 Å for both the lattice atoms and hydrogen. The width of the dividing slab, Δr, is chosen to be equal to the maximum step size to ensure that the hydrogen atom cannot traverse the dividing slab without entering its volume at least once.

To increase convergence speed, subsequent to the Markov step described above, K damped trajectory cycles are executed holding the hydrogen atom stationary.[20,28,31] In this procedure, the kinetic energy of each lattice atom is set to zero, and the classical Hamiltonian equations of the motion for the lattice atoms are integrated until the total potential energy attains a minimum. This is defined to be one trajectory cycle. Subsequent cycles are executed by repeating the above procedure starting with the lattice configuration achieved in the previous cycle. The use of this technique causes the Markov steps to be taken in the near vicinity of the minimum-energy pathway which significantly reduces the computational time required to achieve convergence.

Since the system potential is independent of mass, the actual execution of the above procedure can be greatly facilitated by integrating the classical motion equations with the mass of all atoms set to 1.0 amu. In addition, we may employ a very large integration step size since we need not be concerned with the conservation of energy. The use of these two techniques significantly reduces the computational time required for convergence.

A partial minimization of $F(T)$ is carried out by computing the flux through a set of spherical dividing slabs with radii of ($R = 0.05jd$) for $j = 1, 2, 3, ..., 20$, where d is the total diffusion distance measured from the initial adsorption site. After the initial state is determined, the entire system is allowed to relax to the nearest potential minimum using a set of 100 damped trajectory cycles. The numerical evaluation of the flux begins at this point. The variational transition-state theory method assumes that $k(T)$ can be accurately replaced with $F_{min}(T)$, where $F_{min}(T)$ is the minimum flux obtained in the variational adjustment of the dividing slab.

III. Potential Energy Surfaces

The potential surface is identical to that we have previously employed to study hydrogen atom diffusion in perfect fcc Xe matrices.[29] The total potential for the hydrogen atom/matrix system is assumed to be the separable sum given by eq 6. The potential for the lattice interaction is

$$V_M = \sum_{\substack{i=1 \\ i \neq k}}^{N} V_{ij}(r_{ij}) \tag{21}$$

where r_{ij} is the distance between lattice atoms i and j, and N is the total number of the lattice atoms in the matrix model. k is the index number of vacant sites in the crystal. V_{ij} is taken to be a Morse potential with a cutoff radius, $r_{ij} = R_c$, given by

$$V_{ij} = D[\exp\{-2\alpha(r_{ij} - r_0)\} - 2\exp\{-\alpha(r_{ij} - r_0)\}] \quad \text{for } r_{ij} \leq R_c$$

$$V_{ij} = 0 \qquad \text{for } r_{ij} > R_c \tag{22}$$

The intermolecular potential for the hydrogen−lattice interaction is also assumed to have the pairwise form

$$V_I = \sum_{\substack{i=1 \\ i \neq k}}^{N} V_{iH}(r_{iH}) \tag{23}$$

where r_{iH} is the distance between lattice atom i and the hydrogen atom. The V_{iH} term is taken to be a Lennard−Jones(12,6) potential given by

$$V_{iH} = \epsilon\{(\sigma/r_{iH})^{12} - 2(\sigma/r_{iH})^6\} \tag{24}$$

The assumption of pairwise interactions is common in treating substrate/matrix interactions. Howard *et al.*[34] have shown that the potential for the Ar + Ar_2 system in the gas phase may be accurately represented by a pairwise sum. They found that the inclusion of three-body triple dipole terms gave essentially the same dynamical results. In addition, they found no significant differences between the results obtained with simple Morse potentials and those calculated using the more accurate Morse−spline−van der Waals potential obtained from scattering data reported by Parson *et al.*[35]

Fraenkel and Haas[36] have used Lennard-Jones pairwise potentials to examine the trapping of SF_6 in Ar and Xe matrices. In these studies, SF_6 was treated as a single particle. Guo and Thompson[30] used Lennard-Jones (12,6) potentials to investigate atomic diffusion in Ar and Xe matrices. In their calculations, the potential parameters were obtained from simple arithmetic and geometric mean combining rules using data reported by Allen and Tildesley[37] and by Ashcroft and Mermin.[38] This procedure yields a Xe lattice constant of 6.325 Å, which is 0.085 Å greater than the measured value reported by Kane[39] and 0.202 Å larger than the more recent result obtained by Mason and Rice.[40] For the Xe−H interaction, the combining rules predict an equilibrium separation of 3.815 Å and a well depth of 0.003 85 eV.

In the present study, we have obtained the potential parameters for the Xe lattice required by eqs 21 and 22 from the experimental scattering data reported by Barker *et al.*[41] The use of these values in eq 22 has been shown[20] to yield a Xe lattice constant of 6.131 Å, in good agreement with the value reported by Mason and Rice.[40] The Xe heat of sublimation computed from the 666-atom lattice model described above is 13.4% larger than the value reported by Kane.[39]

The potential parameters for the Xe−H interaction required in eqs 23 and 24 were obtained by fitting the results of *ab initio* calculations.[29] A double-ζ (DZ) basis set combined with the pseudopotential for the xenon core developed by Wadt and Hay[42] was employed. The Xe−H equilibrium interatomic distance and the potential well depth relative to the separated atoms were computed at the Hartree−Fock (HF), and Möller−Plesset second-order (MP2) and fourth-order (MP4) perturbation theory levels using GAUSSIAN 92.[43] The results show that the Xe−H doublet is unbound at the HF level of theory. At the MP2 level, it is very weakly bound with a well depth of 0.000 272 eV at an equilibrium Xe−H separation of 4.5903 Å. At the equilibrium separation predicated by the MP2 calculations, MP4 calculations with all single, double, triple, and quadruple excitations included predict a well depth of 0.000 189 eV. These latter results are the ones employed for the Xe−H interactions in the present study. The potential parameters for all interactions are given in Table 1.

TABLE 1: Pairwise Potential Parameters

Xe−Xe[a]	
D	0.02421405 eV
α	1.4676000 Å^{-1}
r_0	4.36230 Å
R_c	7.000 Å
Xe−H[b]	
ϵ	0.000188 eV
σ	4.5903 Å
R_c	7.000 Å

[a] Taken from ref 20. [b] Taken from ref 29.

The present *ab initio* calculations suggest that the use of combining rules to obtain mixed interactions for atoms as different as xenon and hydrogen may be a flawed procedure. The equilibrium separation given by the MP2 calculations is 0.775 Å larger than that obtained by Guo and Thompson[30] using simple combining rules. The Xe−H well depth given by the MP4 calculations is only 4.9% of that predicted by use of combining rules.[30] This type of result does not seem to be dependent upon the data set employed with the combining rules. We have previously obtained results[44] very similar to those reported by Guo and Thompson[30] using combining rules with pairwise data reported by Gunde *et al.*[45] With this data set, the calculated Xe−H equilibrium separation is 3.802 Å. This result is in good accord with the value obtained by Guo and Thompson,[30] but it is 0.788 Å below the MP2 *ab initio* result. The calculated[44] Xe−H well depth of 0.002 12 eV is still much greater than that predicted by the MP4 *ab initio* calculations.

All of the above calculations are for gas-phase interactions. As such, the effects of the matrix environment upon the potentials are ignored. The level of accuracy of the pairwise form of eqs 21−24 for matrix processes is unknown. As a result, the extent to which our model corresponds to the experimental systems is very uncertain. Our previous studies of hydrogen atom diffusion in perfect fcc matrices[29] suggest that the calculated diffusion coefficients may not be too sensitive to the actual choice of potential parameters. Diffusion coefficients at 40 K calculated using the *ab initio* potential described above and the one obtained using combining rules with data reported by Gunde *et al.*[45] differed by only 9%.

IV. Results and Discussion

We have computed average hydrogen atom diffusion rates at temperatures between 12 and 80 K in xenon matrices containing 1.37 and 4.12% vacancies in the 364-atom P and Q zones of the model lattice. This corresponds to 5 and 15 vacancy sites, respectively. These choices are arbitrary, but not without reason. The lower percentage corresponds roughly to the actual experimental lattices generated by vapor deposition methods[25,26] while the higher value allows us to examine the expected behavior for an upper limit case.

The Markov walk/damped trajectory procedure described above is found to converge at a rate much faster than normally

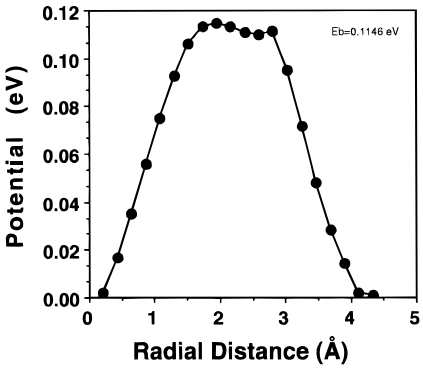

Figure 1. Potential energy barrier for hydrogen atom diffusion in a Xe matrix with 1.37% vacant sites. The plotted points are the minimum crossing potentials obtained in the Markov/damped trajectory walk of 75 000 moves. The abscissa gives the radial diffusion distance covered.

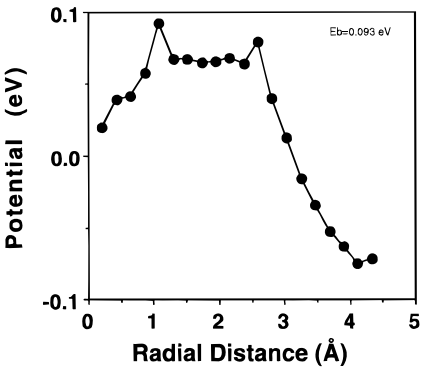

Figure 2. Potential energy barrier for hydrogen atom diffusion in a Xe matrix with 4.12% vacant sites. The plotted points are the minimum crossing potentials obtained in the Markov/damped trajectory walk of 50 000 moves. The abscissa gives the radial diffusion distance covered.

seen in the calculation of diffusion rates using classical variational transition-state theory methods.[28,29] Convergence of the diffusion rates for oxygen atoms in xenon matrices[28] was achieved in 5×10^4 steps with the Markov/damped trajectory procedure. In contrast, it was not possible to obtain convergence with 10^6 steps by employing classical variational transition-state methods with Markov moves alone. In the present calculations, convergence is obtained with $0.75-2.0 \times 10^5$ Markov/damped trajectory steps.

Equation 6 predicts a significant potential barrier to the diffusion of hydrogen atoms within the matrix cage. For the case of a perfect fcc lattice with the atoms frozen in their equilibrium positions, the barrier for straight-line diffusion of hydrogen from one adsorption site to another is 2.855 eV. As expected, the barrier crest occurs at a distance $d/2$ from the initial adsorption site. This barrier increases as ϵ and σ in eq 23 increase. Obviously, no diffusion will occur at cryogenic temperatures with a barrier of this magnitude. However, when the lattice is permitted to relax in the potential field of the hydrogen atom and the phonon modes of the lattice are allowed to contribute to the diffusion process, the barrier decreases to 0.121 eV.[29]

In the present case, dynamic barriers have been determined by recording the minimum system potential for each of the dividing slabs obtained from hydrogen-atom crossings observed during the Markov/damped trajectory walk. Typical results are shown in Figures 1 and 2. Figure 1 shows a typical barrier for a system with 1.37% vacancies, and Figure 2 shows the corresponding result for a lattice containing 4.12% vacancies. With 1.37% vacancies, the relaxation of the lattice reduces the energy barrier to 0.1146 eV, 0.0064 eV lower than that for the no vacancy case. When the vacancy percentage reaches 4.12%, the barrier shape shows a significant loss of symmetry. The example seen in Figure 2 illustrates this point. In this case, the dynamic barrier is reduced to 0.093 eV, 0.0216 eV below that for the lattice with 1.37% vacancies. We see also that the barrier crest shifts to about 1.2 Å. The fact that lattice vacancies lower the dynamic barrier to diffusion indicates that such vacancies will have a profound influence on the hydrogen atom diffusion rates.

TABLE 2: Classical Diffusion Rates for Hydrogen Atoms

T (K)	% vacancies	M[a]	E_b[b] (eV)	D[c] (cm^2/s)
40	0.00[d]	75 000	0.1210	2.15×10^{-15}
40	1.37	75 000	0.1153	(5.71 ± 1.04)[e] $\times 10^{-14}$ [e]
12	4.12	75 000		3.06×10^{-12}
40	4.12	50 000	0.093	1.45×10^{-10}
80	4.12	40 000		3.97×10^{-4}

[a] Number of moves in the Markov/damped trajectory walk. [b] Potential barrier height. [c] Classical diffusion coefficients. [d] Reference 29. [e] One sigma limit of statistical uncertainty in averaging over the lattice vacancy sites.

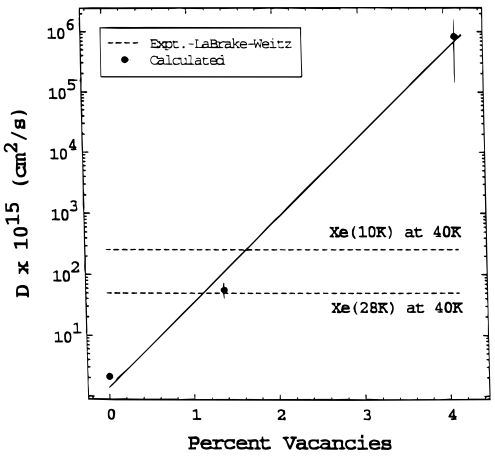

Figure 3. Variation of the computed hydrogen atom diffusion coefficient with percentage of vacant xenon sites at 40 K. The error bars represent one sigma limit of statistical uncertainty in averaging over the vacancies sites. The horizontal dashed lines are the experimental values reported by LaBrake and Weitz in ref 26 for the matrices indicated in the figure.

Hydrogen atom diffusion rates are computed using eqs 1 and 13 with a Markov walk/damped trajectory procedure. The average hydrogen atom diffusion rates in Xe matrices with 1.37 and 4.12% vacancies are given in Table 2. In each case, the results are obtained by averaging five different calculations each with a different set of vacancy sites. At 40 K, the root-mean-square deviation of the results from the mean corresponds to a statistical uncertainty of ±18%. The hydrogen atom diffusion rate in a lattice with 1.37% vacancies is a factor of 26.6 faster than that for the perfect fcc crystal, while the corresponding diffusion barrier is 4.63% lower. The diffusion rate with 4.12% vacancies is several orders of magnitude faster than that in the perfect crystal, and the diffusion barrier is lowered 0.028 eV relative to the perfect fcc lattice. Because of the small mass of hydrogen, tunneling processes would be expected to make an important contribution to diffusion at low temperatures. Perry *et al.*[29] found that, at temperatures approaching 12 K, diffusion occurs almost exclusively *via* tunneling. At 40 K and above, however, tunneling was found to be negligible.

The decrease of the diffusion barrier with increasing vacancy percentage suggests that the diffusion rate should vary exponentially with vacancy percentage. Figure 3 shows a semilog plot of the calculated hydrogen atom diffusion coefficients in a

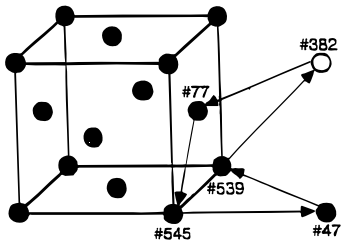

Figure 4. Typical lattice atom motion occurring during the first 200 000 Markov steps in the Monte Carlo calculation. At time $t = 0$, site 382 is vacant. The diffusion of the vacancy as shown by the solid arrows produces a vacancy at site 77 so that the overall result is a diffusion of the vacancy from site 382 → site 539 → site 47 → site 545 → site 77.

xenon matrix as a function of the percentage of vacant sites in the lattice. The near linearity of this plot indicates that the dependence is well described as exponential. A least-squares fit to the data yields

$$D(T{=}40\text{ K}) = 0.145 \times 10^{-15} \exp[1.381p] \quad \text{cm}^2/\text{s} \qquad (25)$$

where D and p are the diffusion coefficient and the vacancy percentage, respectively. This exponential dependence will obviously break down for increasingly large value of p. However, when the vacancy percentage is 5% or less, it appears to be accurate. This increase in diffusion rate is a consequence of a general lattice expansion produced by the vacancies. The expanded lattice provides lower energy pathways for hydrogen atom diffusion to adjoining sites. This expansion mechanism is quite different from one that has the diffusion coefficient increasing because of migration through large "holes" created by the site vacancies.

LaBrake and Weitz[26] have measured hydrogen atom diffusion coefficients in vapor-deposited xenon matrices at 40 K. They used 193 nm photolysis of HBr to produce hydrogen atoms whose concentration was monitored using laser-induced emission from xenon−hydrogen exciplexes. When a xenon matrix vapor deposited at 10 K, denoted Xe(10 K), was maintained at 10 K, the hydrogen-atom concentration remained unchanged over a 5 day period. Thus, the diffusion coefficient at 10 K in Xe(10 K) is effectively zero. When the temperature of the Xe(10 K) matrix is increased to 40 K, hydrogen diffusion is observed with an estimated diffusion coefficient of 2.6×10^{-13} cm^2/s. In contrast, when a Xe(28 K) matrix is warmed to 40 K, a diffusion coefficient of 5.0×10^{-14} cm^2/s is obtained. LaBrake and Weitz[26] suggested that this difference is due to the presence of a larger number of imperfections in the lattice deposited at 10 K which are not later annealed at 40 K. This view implicitly assumes that the larger number of vacancies present in the Xe(10 K) lattice will lead to a larger hydrogen atom diffusion coefficient.

The data given in Table 2 and in Figure 3 support the interpretation advanced by LaBrake and Weitz.[26] Equation 25 shows that the diffusion coefficient will indeed increase rapidly with an increase in the number of vacant lattice sites. The horizontal lines shown in Figure 3 are the measured diffusion coefficients[26] in Xe(10 K) and Xe(28 K) lattices. The intersection of these lines with the calculated curve indicates that there are 1.76 and 1.15% vacancies in the experimental Xe(10 K) and Xe(28 K) matrices, respectively.

It is important to note that the calculations show that the vacancy sites are mobile. A typical example is shown in Figure 4 for the case of a xenon lattice at 40 K containing 1.37% vacancies. The figure illustrates the mobility of one of these vacancies, no. 382, during the initial 200 000 Markov steps.

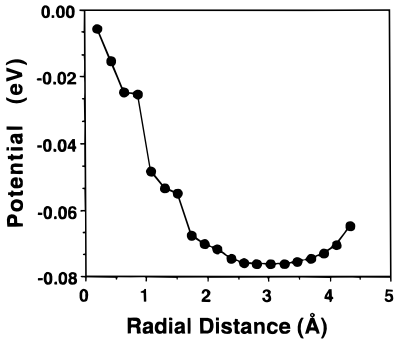

Figure 5. Example of the variation of the potential energy barrier for hydrogen-atom diffusion in a Xe matrix with 1.37% vacant sites subsequent to vacant site diffusion after 200 000 Markov/damped trajectory steps. The plotted points are the minimum crossing potentials obtained in the Markov/damped trajectory walk. The abscissa gives the radial diffusion distance covered.

As can be seen, five translations of this vacancy occur during this period. These translations are induced by the hydrogen atom diffusion which causes the lattice to shift toward a more thermodynamically stable configuration.

The translation of site vacancies can significantly affect the hydrogen-atom diffusion rate since the process alters the potential barrier to diffusion. Figure 5 illustrates this point for a Xe lattice with 1.37% vacant sites. Initially, the diffusion barrier is that shown in Figure 1. After 200 000 Markov steps have been executed, the variation of the system potential between the initial and final absorption sites is that shown in Figure 5. Obviously, the barrier to diffusion has completely vanished. More detailed investigation demonstrates that this drastic alteration of diffusion barrier is the result of vacancy site mobility. Our studies show that the propensity for vacant site mobility increases as the total number of vacancies increases.

Qualitatively, it is clear that vacant site mobility will increase the hydrogen atom diffusion rate since the process lowers the diffusion barrier. Since the canonical Markov walk and damped trajectory calculations are thermodynamically based, we cannot determine the time scale for vacant site mobility from the present calculations. Consequently, it is not possible for us to quantitatively determine the effect of such mobility on the hydrogen atom diffusion rates in imperfect xenon crystals. For this reason, the diffusion coefficients listed in Table 2 should be regarded as lower limits for a system whose potential is described by eq 6. For the same reason, the percentage of vacancies in the Xe(10 K) and Xe(28 K) experimental matrices[26] predicted from Figure 3 and eq 25 are upper limits.

V. Summary

Using a pairwise Xe/H interaction potential obtained from the results of MP4(SDTQ) calculations, thermal diffusion rates of hydrogen atoms in an imperfect face-centered-cubic xenon lattice containing n vacancies have been computed using classical variational transition-state theory. Convergence of the required integrals is achieved by combining importance sampling and a damped trajectory procedure with the standard Markov walk. The variational flux through a spherical dividing surface is minimized as a function of radius of the dividing surface.

The potential barriers to diffusion have been determined by recording the minimum system potential observed upon hydrogen atom crossing on each of the dividing surfaces during the damped trajectory/Markov walk. Typical results show that the presence of 1.4% vacant lattice sites lowers the diffusion barrier by about 0.006 eV relative to the perfect fcc crystal system.

The computed values of the hydrogen atom diffusion coefficients at 40 K indicate that, over the range of vacancies

considered, the diffusion coefficients increase exponentially with the percentage of lattice vacancies. Comparison of the predicted diffusion rates with the experimental values reported by LaBrake and Weitz[26] in vapor-deposited xenon matrices suggests that the Xe lattices deposited at 10 and 28 K have about 1.8 and 1.2% vacant sites, respectively.

The calculations show that the lattice vacancies are mobile. This translation of site vacancies can significantly affect the hydrogen atom diffusion rate since the process lowers the potential barrier to diffusion. Our studies show that the propensity for vacant site mobility increases as the total number of lattice vacancies increases. Although it is clear that vacant site mobility will increase the hydrogen atom diffusion rate, the present calculations do not permit the magnitude of this increase to be determined. This is a consequence of the fact that the canonical Markov walk and damped trajectory calculations are thermodynamically based. Therefore, we cannot determine the time scale for vacant site mobility from the present calculations. For this reason, the diffusion coefficients reported here are lower limits for a system whose potential is described by eq 6. For the same reason, the vacancy percentage predicted for the experimental Xe(10 K) and Xe(28 K) matrices are upper limits for the potential surface used in the present calculations.

The calculated hydrogen atom diffusion coefficients in Xe at 40 K vary from 2.15×10^{-15} cm^2/s for a perfect lattice to 1.45×10^{-10} cm^2/s for a lattice containing 4.12% vacancies. The statistical error present in these results is about $\pm 18\%$. However, lack of knowledge of the true system potential makes the accuracy of the computed coefficients very uncertain.

Acknowledgment. We are pleased to acknowledge financial support from the National Science Foundation under Grant CHE-9211925.

References and Notes

(1) Baldeschwieler, J. D.; Pimentel, G. C. *J. Chem. Phys*. **1960**, *33*, 1008.
(2) Hall, R. T.; Pimentel, G. C. *J. Chem. Phys*. **1963**, *38*, 1889.
(3) Chapman, O. L.; McIntosh, C. L.; Pacansky, J. *J. Am. Chem. Soc*. **1973**, *95*, 244.
(4) Squillacote, M.; Sheridan, R. S.; Chapman, O. L.; Anet, F. A. L. *J. Am. Chem. Soc*. **1975**, *97*, 3244.
(5) Serralach, A.; Meyer, R. *J. Mol. Spectrosc.* **1976**, *60*, 246.
(6) Frei, H.; Ha, T. K.; Meyer, R.; Günthard, Hs. H. *Chem. Phys*. **1977**, *25*, 271.
(7) (a) Pertillä, M.; Murto, J.; Kivinen, A.; Turunen, K. *Spectrochim. Acta* **1978**, *34A*, 9. (b) Pertillä, M.; Murto, J.; Nalonen, L. *Spectrochim. Acta* **1978**, *34A*, 469.
(8) Pourcin, J.; Davidovics, G.; Bodot, H.; Abouaf-Marguin, L.; Gauthier-Roy, B. *Chem. Phys. Lett.* **1980**, *74*, 147.
(9) Bendereskii, A. V.; Wight, C. A. *J. Phys. Chem*. **1996**, *100*, 14958.
(10) Dubs, M.; Ermanni, L.; Günthard, Hs. H. *J. Mol. Spectrosc*. **1982**, *91*, 458.
(11) Felder, P.; Günthard, Hs. H. *Chem. Phys*. **1984**, *85*, 1.
(12) Gunde, R.; Günthard, Hs. H. *Chem. Phys*. **1987**, *111*, 339.
(13) Gunde, R.; Ha, T. K.; Günthard, Hs. H. *Chem. Phys*. **1990**, *145*, 37.
(14) Gunde, R.; Heller, H. J.; Ha, T. K.; Günthard, Hs. H. *J. Phys. Chem*. **1991**, *95*, 2802.
(15) Hauge, R. H.; Gransden, S.; Wang, J.; Margrave, J. L. *J. Am. Chem. Soc*. **1979**, *101*, 6950.
(16) Frei, H.; Fredin, L.; Pimentel, G. C. *J. Chem. Phys*. **1981**, *74*, 397.
(17) Knudsen, A. K.; Pimentel, G. C. *J. Chem. Phys*. **1983**, *78*, 6780.
(18) Frei, H.; Pimentel, G. C. *J. Chem. Phys*. **1983**, *78*, 3698.
(19) Frei, H. *J. Chem. Phys*. **1983**, *79*, 748.
(20) Raff, L. M. *J. Chem. Phys*. **1990**, *93*, 3160.
(21) Agrawal, P. M.; Thompson, D. L.; Raff, L. M. *J. Chem. Phys*. **1994**, *101*, 9937.
(22) Agrawal, P. M.; Thompson, D. L.; Raff, L. M. *J. Chem. Phys.* **1995**, *102*, 7000.
(23) Feld, J.; Kunttu, H.; Apkarian, V. A. *J. Chem. Phys*. **1990**, *93*, 1009.
(24) Lawrence, W. G.; Apkarian, V. A. *J. Chem. Phys*. **1992**, *97*, 6199.
(25) Krueger, H.; Weitz, E. *J. Chem. Phys*. **1992**, *96*, 2846.
(26) LaBrake, D.; Weitz, E. *Chem. Phys. Lett*. **1993**, *211*, 430.
(27) Misochko, E. Ya.; Benderskii, V.; Wight, C. A. *J. Phys. Chem*. **1996**, *100*, 4496.
(28) Ford, M. B. B.; Foxworthy, A. D.; Mains, G. J.; Raff, L. M. *J. Phys. Chem*. **1993**, *97*, 12134.
(29) Perry, M. D.; Mains, G. J.; Raff, L. M. *J. Phys. Chem*. **1994**, *98*, 13766.
(30) Guo, Y.; Thompson, D. L. *J. Chem. Phys*. **1995**, *103*, 9024.
(31) Raff, L. M. *J. Chem. Phys*. **1995**, *97*, 7459.
(32) Riley, M. E.; Coltrin, M. E.; Diestler, D. J. *J. Chem. Phys*. **1988**, *88*, 5934.
(33) Agrawal, P. M.; Thompson, D. L.; Raff, L. M. *J. Chem. Phys*. **1989**, *91*, 6463.
(34) Howard, R. E.; Roberts, R. E.; DelleDonne, M. J. *J. Chem. Phys*. **1976**, *65*, 3067.
(35) Parson, J. M.; Siska, P. E.; Lee, Y. T. *J. Chem. Phys.* **1972**, *56*, 1511.
(36) Fraenkel, R.; Hass, Y. *J. Chem. Phys*. **1994**, *100*, 4324.
(37) Allen, M. P.; Tildesley, D. J. *Computer Simulation of Liquids*; Clarendon: Oxford, 1987.
(38) Ashcroft, N. W.; Mermin, N. D. *Solid State Physics*; Saunders College: Philadelphia, 1976.
(39) Kane, B. G. *J. Chem. Phys*. **1939**, *7*, 603.
(40) Mason, E. H.; Rice, W. E. *J. Chem. Phys*. **1954**, *22*, 843.
(41) Barker, J. A.; Watts, R. O.; Lee, K.; Schafer, T. P.; Lee, Y. T. *J. Chem. Phys.* **1974**, *61*, 3081.
(42) Wadt, P. J.; Hay, W. R. *J. Chem. Phys*. **1985**, *82*, 270.
(43) Frisch, M. J.; Trucks, G. W.; Head-Gordon, M.; Gill, P. M.; Wong, P. M. W.; Foresman, J. B.; Johnson, B. G.; Schlegel, H. B.; Robb, M. A.; Replogle, E. S.; Gomperts, R.; Andres, J. L.; Raghavachari, K.; Binkley, J. S.; Gonzales, C.; Martin, R. L.; Fox, D. J.; Defrees, D. J.; Baker, J.; Stewart, J. J. P.; Pople, J. A. *Gaussian 92*, Revision A; Gaussian, Inc.: Pittsburgh, PA, 1992.
(44) Raff, L. M. *J. Chem. Phys*. **1991**, *95*, 8901.
(45) Gunde, R.; Gelder, P.; Günthard, Hs. H. *Chem. Phys*. **1982**, *64*, 313.